

# Three-Dimensional Fully Interlaced Woven Microstrip-Fed Substrate Integrated Waveguide

Leticia Alonso-González\*, Samuel Ver-Hoeye,  
Miguel Fernández-García, and Fernando Las-Heras

**Abstract**—A three-dimensional fully interlaced woven microstrip-fed substrate integrated waveguide has been designed, manufactured and experimentally validated. The waveguide has been conceived based on the conventional substrate integrated waveguide (SIW) technology and works in a range of frequencies between 7.5 GHz and 12 GHz. The SIW structure is suitable to be translated into different equivalent woven structures depending on the characteristics of the employed threads, as it has been presented in previous works. In this work, a structure based on rigid weft threads has been employed with the aim of translating both the waveguide and the corresponding SIW to microstrip transitions, into woven patterns and, therefore, achieving the main purpose of a complete integration of the circuit into the textile, avoiding the use of external transitions for its validation. Consequently, three prototypes, using three different lengths, have been manufactured and experimentally characterised, and the theoretically predicted behaviour of the prototypes has been experimentally verified.

## 1. INTRODUCTION

During the last years, there has been increasing interest in microwave textile integrated circuits (TIC) due to the possibility of their integration in clothing or technical textiles and the development of conformable structures such as upholsteries. In the literature, a variety of solutions to develop TIC has been proposed. For instance, embroidery techniques represent a full integration of the circuit into the textile; nevertheless, it does not allow multilayered designs [1–6]. On the contrary, non-wovens are fabric-like materials made from different kinds of fibers, bonded together by different procedures, leading to materials such as felt which are neither woven nor knitted [7–9]. For this reason, a multilayered non-woven can be manufactured, although different subsequent procedures may be required to structure and provide it with the desired electromagnetic behaviour. Another alternative to develop TIC is the use of applique processes, which consist of attaching various textile materials employing different alternatives such as sewing, adhesive or gluing procedures [10–15], although the different procedures to manufacture the final prototype lead to the difficulty of its large scale production. However, one of the most cited alternatives to develop TIC is inkjet printed patterns over textile substrates [16–20]. The use of the printing techniques — screen printing or inkjet printing — for the realisation of conductive patterns over textile substrates presents several advantages regarding the possibility of achieving complex details in the designs. Nevertheless, the requirement of an interface layer to deal with the uneven substrates represents an additional subprocess which costs time during the manufacturing of the prototypes.

Furthermore, more recently, SIW structures have been found very interesting to be integrated in textile, and several solutions have been proposed in the literature for this purpose. As an example, the conductive and dielectric elements of a textile SIW structure can be achieved using electrically

---

*Received 2 April 2018, Accepted 31 May 2018, Scheduled 8 August 2018*

\* Corresponding author: Leticia Alonso-González (lalonso@tsc.uniovi.es).

The authors are with the Signal Theory and Communications Area, Department of Electrical Engineering, University of Oviedo, Campus Universitario de Viesques, Edificio Polivalente, Despacho 0.8.07, Gijón E-33203, Spain.

conductive and dielectric fabrics, respectively, whereas the conductive vias can be achieved employing conductive threads [21], eyelets [22–26] or conductive cylindrical wires [27]. However, the before mentioned alternatives to develop textile SIW prototypes are not completely integrated in textile, as they require eyelets or wires, and require several processes to be manufactured. For this reason, weaving technology has been found to be an interesting option to deal with the beforementioned problems.

A woven structure can be divided into two different sets of threads, the warp and the weft threads [28]. While the warp threads are previously assembled in the loom, the weft threads are successively inserted in the loom to create the woven structure. Consequently, depending on the characteristics of the materials from which the threads have been extruded, and the manufacturing procedure of the threads — whether they are multifilaments or monofilaments — the threads will tend to be flexible or rigid. In [29], a TIW using rigid warp multifilament threads has been developed, then, the conductive vias are achieved using different patterns of the flexible weft threads. For its experimental validation, a pair of 3D-printed TIW to rectangular waveguide transitions have been designed and manufactured, because the textile prototype only includes the waveguide.

However, the TIW proposed in this paper is totally different from the TIW already presented in [29]. In this paper, a microwave microstrip-fed fully TIW is proposed, avoiding the necessity of manufacturing a pair of 3D-printed TIW to rectangular waveguide transitions, and consequently achieving the main purpose, which is a complete integration of the circuit into the textile structure. For this purpose, the three-dimensional woven structure requires an additional layer of weft threads and its corresponding binders, which are subsequently removed in order to achieve the TIW to microstrip transitions. Moreover, in this paper, because the warp threads are flexible, they provide the possibility of creating different warp patterns. As the weft threads are rigid, a constant height of the textile substrate can be achieved [30], leading to a better performance of the TIW.

The paper is organised as follows. In Section 2, the structure of the TIW will be presented. In Section 3, the employed conductive materials will be explained. In Section 4, the employed dielectric materials will be analysed. In Section 5, the design of the TIW and subsequent translation into woven prototypes will be detailed. In Section 6, the design of the TIW to microstrip transition will be explained. In Section 7, the simulations will be presented. In Section 8, the fabrication process will be explained. In Section 9, the experimental validation will be presented.

## 2. STRUCTURE OF THE TIW

A three-dimensional microstrip-fed TIW using rigid weft threads is proposed for its single-mode operation at a range of frequencies between 7.5 GHz and 12 GHz. The TIW has been designed using the three-step modelling which has already been discussed in [29] and particularised to two steps in [30] due to the use of monofilaments. Figure 1 represents an overview of the Layers Model (LM) associated with the proposed TIW, the coordinate system, the orientation of the electromagnetic (EM) field and the propagation direction.

The TIW is based on a SIW, then, it can be divided into three different layers, a dielectric layer (whose height is denoted by  $H_{\text{SIW}}$ ) between two conductive plates. The separation between the two

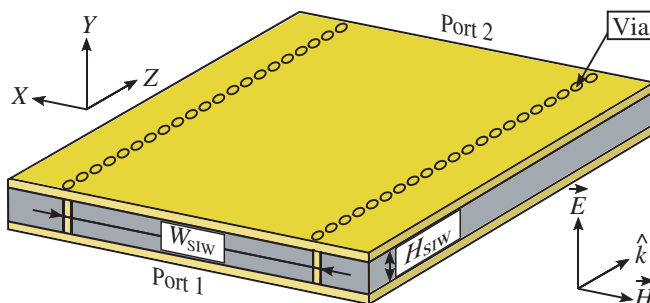


**Figure 1.** Schematic drawing of the proposed TIW, conductive materials (yellow) and dielectric materials (grey).

rows of conductive vias is given by  $W_{SIW}$ , whereas the diameter of each via and the separation between two consecutive vias are given by  $D$  and  $S$ , respectively. The parametric length of the TIW is given by  $L_{SIW}$ .

The proposed TIW is fully integrated in textile; therefore, the conductive and dielectric parts are manufactured using different types of threads. In the proposed TIW, the warp direction coincides with the propagation direction, whereas the weft direction is parallel to the orientation of the magnetic field. Unlike in the case of the TIW presented in [29], where the warp threads remain straight, in this work, the weft threads are the ones which remain straight, then the different warp patterns generate the woven structure. The conductive and dielectric employed materials will be explained in Section 3 and Section 4, respectively.

### 3. CHARACTERISATION OF THE CONDUCTIVE MATERIALS

Electrically conductive *Shieldex 117f17 2-ply* yarns, with 17 filaments per ply and a density of 117 dtex [29] have been used for the weft threads. For simplification, this material will be denoted by *Shx2p*. The threads usually present a circularly shaped cross section; however, when they are in a woven structure, due to the forces actuating between them, the cross section of the multifilament threads can be deformed [31]. The *Shx2p* threads employed in this prototype adopt a Pierce’s elliptic cross section when they are in the woven structure which will be then presented. In addition, electrically conductive *Shieldex 117f17 1-ply* yarns, with 17 filaments per ply and a density of 117 dtex have been used for the warp threads. These threads adopt a circular cross section, then they are not deformed when they are in the woven structure which will be then presented. The cross section approaches and corresponding dimensions of the different conductive threads are summarised in Table 1. The thickness of the silver coating of each filament, for both types of threads, is given by  $T_c = 0.5 \mu\text{m}$ , whereas the total diameter of each filament is given by  $D_f = 31 \mu\text{m}$ , as depicted in Figure 2(a).

**Table 1.** Cross section dimensions of the employed conductive materials.

Material	Thread direction	Cross section	Dimension	Value (mm)
<i>Shx2p</i>	Weft	Pierce	Horizontal semi-axis	0.1
			Vertical semi-axis	0.05
<i>Shx1p</i>	Warp	Circularly	Circumference radius	0.075

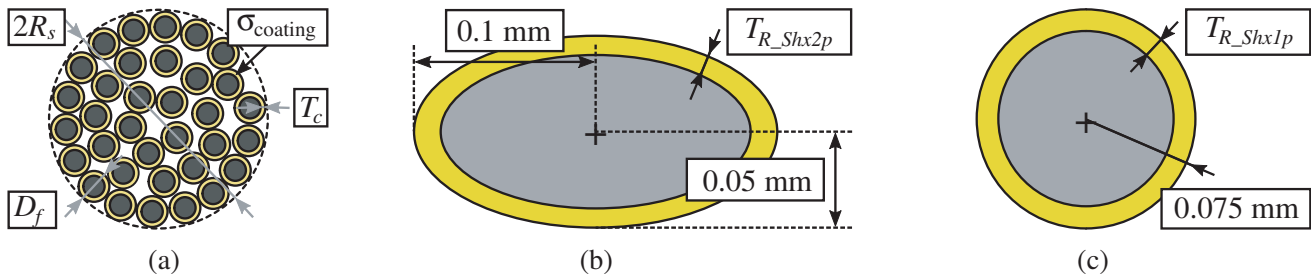


**Figure 2.** Cross section dimensions of the conductive threads. (a) Overview of the multifilament cross section. (b) *Shx2p* threads. (c) *Shx1p* threads.

Following the procedure described in [30], the skin depth effect of both threads has been analysed. First, the skin depth,  $\delta_{Sd}$ , is calculated using the minimum frequency,  $f_{\min} = 7.5 \text{ GHz}$ , applying Eq. (1). As the resistivity of the silver is  $\rho_{\text{Silver}} = 1.59 \cdot 10^{-8} (\Omega\text{m})$ ,  $\delta_{Sd} = 0.7328 \mu\text{m}$ .

$$\delta_{Sd} = \sqrt{\frac{\rho_{\text{Silver}}}{\pi \mu f_{\min}}} \tag{1}$$

Then, the total surface of conductive coating,  $S_c$ , in the  $N_{\text{fil}}$  filaments is calculated using Eq. (2). For  $Shx2p$  threads,  $N_{\text{fil}_Shx2p} = 34$  filaments, consequently,  $S_{c\_Shx2p} = 8.2113 \cdot 10^{-10} \text{ m}^2$ . Alternatively, for  $Shx1p$  threads,  $N_{\text{fil}_Shx1p} = 17$  filaments, therefore,  $S_{c\_Shx1p} = 4.1057 \cdot 10^{-10} \text{ m}^2$ .

$$S_c = \pi N_{\text{fils}} \left( \left( \frac{D_f}{2} \right)^2 - \left( \frac{D_f - T_c}{2} \right)^2 \right) \quad (2)$$

The cross section associated with  $Shx2p$  threads has been approximated by the Pierce's cross section. Therefore, as summarised in Table 1, it is an ellipse whose semi-axes are 0.1 and 0.05 mm, respectively. The total surface of conductive coating,  $S_{c\_Shx2p}$ , can be translated into an equivalent conductive ring whose thickness is given by  $T_{R\_Shx2p}$ , as depicted in Figure 2(b). The effective thickness of the coating ring,  $T_{R\_Shx2p}$ , can be calculated generalising Eq. (2) for the Pierce's cross section, using Eq. (3). Consequently,  $T_{R\_Shx2p} = 1.7632 \text{ } \mu\text{m}$ .

$$\pi \cdot 0.1 \cdot 10^{-3} \cdot 0.05 \cdot 10^{-3} - \pi 10^{-3} (0.1 - T_{R\_Shx2p}) \cdot 10^{-3} (0.05 - T_{R\_Shx2p}) = S_{c\_Shx2p} \quad (3)$$

Because  $T_{R\_Shx2p}$  is greater than  $\delta_{\text{sd}}$ , the  $Shx2p$  thread can be substituted by a completely conductive thread, whose conductivity can be calculated generalising Eq. (4) for the Pierce's cross section, using Eq. (5). Therefore,  $\sigma_{\text{mon}_Shx2p} = 3.2877 \cdot 10^6 \text{ S/m}$ .

$$\sigma_{\text{mon}} = \sigma_{\text{coating}} \frac{\text{coating area}}{\text{cross section area}} = \sigma_{\text{coating}} \frac{S_c}{\pi R_s^2} \quad (4)$$

$$\sigma_{\text{mon}_Shx2p} = \frac{1}{\rho_{\text{Silver}}} \frac{S_{c\_Shx2p}}{\pi \cdot 0.1 \cdot 10^{-3} \cdot 0.05 \cdot 10^{-3}} \quad (5)$$

Alternatively, the cross section associated with  $Shx1p$  threads has been approximated by the circular cross section. Therefore, as summarised in Table 1, it is circumference whose radius is 0.075 mm. The total surface of conductive coating,  $S_{c\_Shx1p}$ , can be translated into an equivalent conductive ring whose thickness is given by  $T_{R\_Shx1p}$ , as depicted in Figure 2(c). The effective thickness of the coating ring,  $T_{R\_Shx1p}$ , can be calculated particularising Eq. (2) for this circularly cross section, using Eq. (6). Consequently,  $T_{R\_Shx1p} = 0.8764 \text{ } \mu\text{m}$ .

$$\pi \cdot 0.075 \cdot 10^{-3} \cdot 0.075 \cdot 10^{-3} - \pi 10^{-3} (0.075 - T_{R\_Shx1p}) \cdot 10^{-3} (0.075 - T_{R\_Shx1p}) = S_{c\_Shx1p} \quad (6)$$

Because  $T_{R\_Shx1p}$  is greater than  $\delta_{\text{sd}}$ , the  $Shx1p$  thread can be substituted by a completely conductive thread, whose conductivity can be calculated particularising Eq. (4) for this circular cross section, using Eq. (7). Therefore,  $\sigma_{\text{mon}_Shx1p} = 1.4612 \cdot 10^6 \text{ S/m}$ .

$$\sigma_{\text{mon}_Shx1p} = \frac{1}{\rho_{\text{Silver}}} \frac{S_{c\_Shx1p}}{\pi \cdot 0.075 \cdot 10^{-3} \cdot 0.075 \cdot 10^{-3}} \quad (7)$$

#### 4. CHARACTERISATION OF THE DIELECTRIC MATERIALS

For the dielectric parts of the prototype, two different types of thread have been employed. For the warp threads, uncoated polyethersulfone (PES) monofilament has been used. For the weft threads, uncoated polyethylene-terephthalate (PET) monofilament has been employed. For simplification, the PES warp threads and PET weft threads will be denoted by  $\text{PES}_{\text{warp}}$  and  $\text{PET}_{\text{weft}}$ , respectively.

The characteristic parameters of the employed materials at the working range of frequencies are defined for the Monofilament Model (MM), as the threads are monofilaments, as follows. The relative permittivities of the PET and PES are  $\varepsilon_{\text{mon\_PET}} = 3.4$  and  $\varepsilon_{\text{mon\_PES}} = 3.7$ , respectively. The loss tangents associated with the PES and PET are  $\tan(\delta)_{\text{mon\_PES}} = 0.01$  and  $\tan(\delta)_{\text{mon\_PET}} = 0.001$ , respectively [32, 33]. The before mentioned characteristic parameters are summarised in Table 2.

For both  $\text{PES}_{\text{warp}}$  and  $\text{PET}_{\text{weft}}$  threads, the circular cross section was found to be the best approximation. The dimensions of the cross section of each type of dielectric thread are indicated in Table 3.

According to the procedure referenced in [29, 30] and because the  $\text{PES}_{\text{weft}}$  threads remain straight, the different warp threads will conform the woven structure around the weft threads. The ends per inch

**Table 2.** Characteristic parameters of the employed dielectric materials.

Parameter	PES	PET
Relative permittivity	$\epsilon_{\text{mon\_PES}} = 3.4$	$\epsilon_{\text{mon\_PET}} = 3.7$
Loss tangent	$\tan(\delta)_{\text{mon\_PES}} = 0.01$	$\tan(\delta)_{\text{mon\_PET}} = 0.001$

**Table 3.** Cross section dimensions of the employed dielectric materials.

Material	Thread direction	Cross section	Dimension	Value (mm)
PES <sub>warp</sub>	Warp	Circularly	Radius	0.075
PET <sub>weft</sub>	Weft	Circularly	Radius	0.5

and picks per inch, commonly known as *epi* and *ppi*, parameters employed in both designs are 169.3 and 16.9, respectively, leading to the woven structures which will be explained in detail in Section 5.

Nevertheless, for clarification, the parameters which describe the LM are calculated and presented in this section. Given the *epi* and *ppi* parameters and the dielectric characteristics of the employed materials and following the procedure explained in [29, 30], the equivalent relative permittivity,  $\epsilon_{\text{eq}}$ , has been found very close to 1. It means that even though the woven substrate is composed of materials whose relative permittivities are different from  $\epsilon_{\text{air}}$ , the existence of thick dielectric yarns, placed perpendicularly aligned with the propagation direction, leads to the existence of big air gaps, consequently reducing the value of the equivalent relative permittivity. Using this estimation procedure no more precision can be achieved; however, the design will not be affected by the use of  $\epsilon_{\text{eq}} = 1$ . Analogously, the equivalent loss tangent has been calculated and found to be  $\tan(\delta)_{\text{eq}} = 0.01$  due to the influence of the PES. Moreover, the equivalent electrical conductivity has also been calculated, then,  $\sigma_{\text{eq}} = 5 \cdot 10^5 \text{ S/m}$ .

## 5. DESIGN OF THE WOVEN PROTOTYPE

Once the materials have been characterised and the densities of the woven structure, *epi* and *ppi* parameters, have been defined, a woven design which emulates the structure of a SIW is required. For the conductive plates of the SIW, top and bottom layers, two layers composed of warp and weft conductive threads, have been used. The substrate has been realised using a single layer of dielectric material composed of warp and weft threads. The conductive vias have been emulated using conductive warp threads crossing the prototype from the top to the bottom layer. In the proposed textile structure, the effective diameter of the vias is closely related to the diameter of the conductive warp threads employed to implement the top and bottom conductive layers of the TIW structure. The diameter of these conductive warp threads restricts not only the effective diameter of vias, but also the separation between two consecutive vias,  $S$ , which is also restricted by the diameter of the dielectric weft threads.

The distance between the two rows of conductive vias has been designed to be  $W_{\text{SIW}} = 25 \text{ mm}$ , in order to achieve required cutoff frequency. The separation between two consecutive vias belonging to the same row has been designed to be  $S = 1.5 \text{ mm}$ , whereas the diameter of the conductive vias is  $D = 1.5 \text{ mm}$ . For this reason, different warp patterns have been designed to create the SIW structure, while connecting the different layers of the prototype generalising the equations described in [29] for the different cross sections.

The design of conventional SIW, manufacturable using standard prototyping machines, presents an important difference compared with the design of their analogous TIW. In a SIW, the diameter of the via holes can be increased while keeping the distance between the centres of the via holes as a constant, up to a certain limit. By doing this, the space between two consecutive vias is reduced. However, increasing the effective diameter of the vias can only be achieved by using thicker conductive warp threads, which leads to different consequences. On the one hand, the separation between the vias does not remain constant, but increases, which leads to the increase of the losses. On the other hand, when the diameter

of the vias increases and, consequently, the diameter of the conductive warp threads, these threads become thicker and less flexible, leading to the impossibility of implementing the desired warp patterns. For these reasons, in order to reduce the losses of the woven structure, a possible solution is proposed. The diameter of the thick dielectric weft threads can be reduced, and consequently, the via would keep the same diameter while the distance between two consecutive vias would be reduced. However, the thickness of the woven structure would also be reduced. This consequence could also be solved by employing more interwoven layers of dielectric thinner threads; however, a more complex weaving loom would be required. For the aforementioned reasons, the dimensions of the threads employed to develop the proposed TIW have been chosen in order to achieve a balance between the losses and the required thickness of the structure.

An MM woven structure can be developed to emulate a SIW, as depicted in Figure 3. Figure 3(a) shows a conventional SIW or, equivalently, the LM associated to a TIW. The electric field is vertically oriented, therefore, parallel to the  $Y$ -axis, whereas the magnetic field is parallel to the  $X$ -axis. Consequently, the EM field propagates in  $\hat{k}$  direction from port 1 to port 2. Figure 3(b) depicts the woven translation of the SIW, in which the conductive materials are yellow colored, and the dielectric materials are gray colored. The woven MM structure is composed of three layers of warp threads, a layer of dielectric threads between two layers of conductive materials. The warp threads are parallel to the propagation direction. Then, the woven structure is achieved by weaving different warp patterns around the rigid weft threads. A magnification of the TIW is shown in the bottom right corner of Figure 3(b).

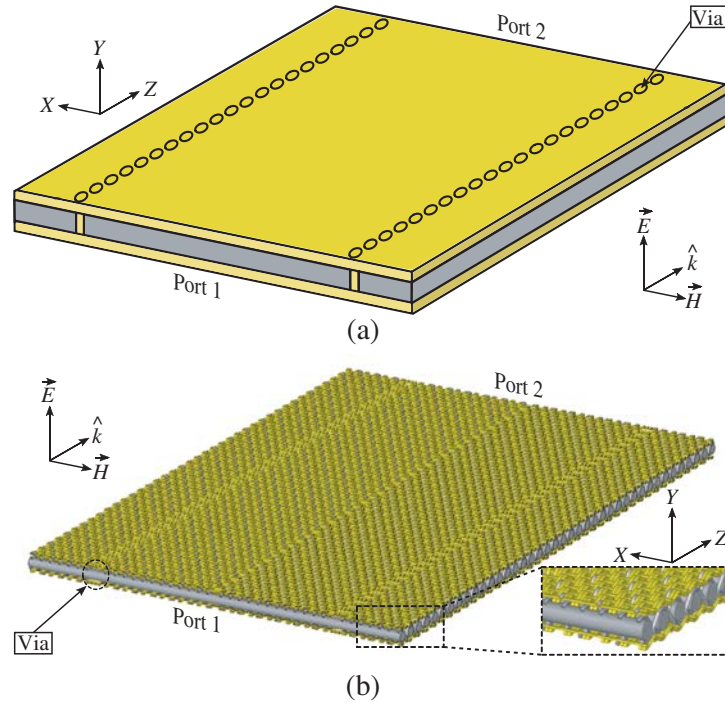


**Figure 3.** General overview of the proposed design. (a) Conventional SIW equivalent to the LM. (b) Proposed woven structure of the TIW and magnification.

Figure 4 depicts different views of the proposed three-dimensional fully interlaced structure and detailed warp patterns [34, 35]. Figure 4(a) represents a general side view of the woven structure in which the height of the prototype,  $H_{\text{SIW}}$ , is indicated. Moreover, the weft ends and warp threads which conform the woven structure are represented, while the conductive warp patterns generate the conductive plates, and the dielectric warp patterns connect the woven substrate. Figure 4(b) depicts the side view of the substrate patterns, which are called binders and are required to connect the three layers of the woven structure with the aim of implementing a compact structure. Figure 4(c) represents

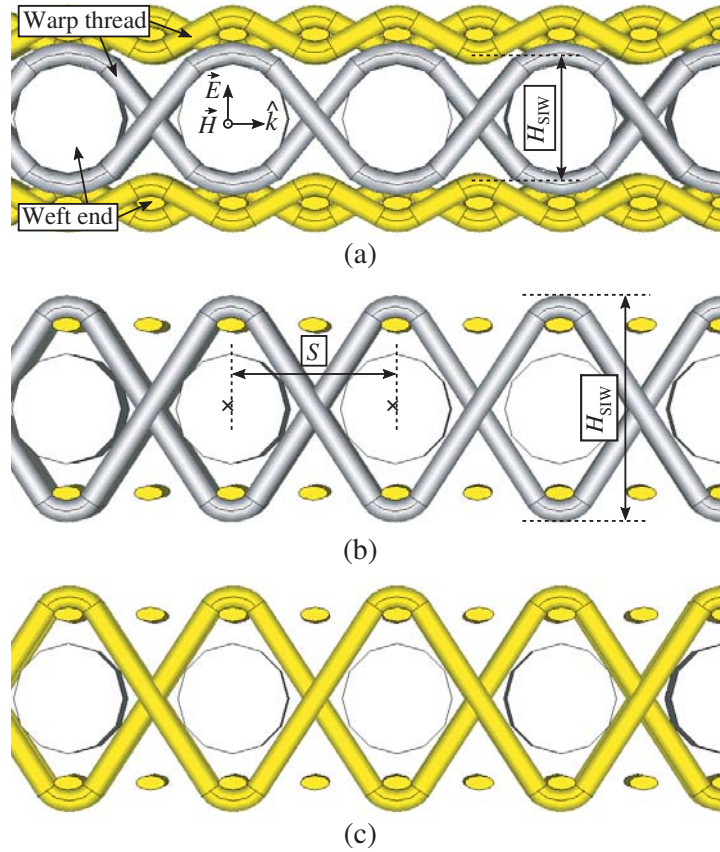


**Figure 4.** MM of the TIW (conductive material is yellow colored and dielectric materials are gray colored). (a) General side view. (b) Side view of the substrate patterns to connect the three layers. (c) Side view of the vias patterns.

the side view of the vias patterns to electrically connect the top and bottom conductive layers.

A general top view and magnification of the woven structure are depicted in Figure 5(a), where the separation between the conductive vias is also detailed. Figure 5(b) represents the front view, or view from the port of the woven structure. Combining the different warp patterns with the weft threads, the before mentioned woven structure presented in Figure 5(b) can be achieved.

## 6. DESIGN OF THE TIW TO MICROSTRIP TRANSITION

For the posterior experimental validation of the prototype, a TIW to microstrip line transition has been designed. As the height of the prototype is given by the width of the dielectric weft threads,  $H_{SIW} = 1\text{ mm}$ . Given the height of the substrate and its equivalent relative permittivity,  $\epsilon_{eq} = 1$ , then the width,  $W_{ML}$ , of a microstrip line, whose characteristic impedance is equal to  $50\ \Omega$ , can be worked out using LineCalc from ADS. Consequently,  $W_{ML} = 5\text{ mm}$ .

The transition is based on a tapered transmission line, as depicted in Figure 6, whose dimensions have been optimised for maximum coupling between the TIW and the microstrip line. Consequently, the dimensions of the taper have been found to be  $W_T = 22\text{ mm}$  and  $L_T = 20\text{ mm}$ .

## 7. SIMULATIONS

The proposed prototype has been electromagnetically analysed using a 3D high frequency simulator with a frequency solver and a tetrahedral mesh. Figure 7 represents the simulated magnitude of the scattering parameters of the equivalent LM (including the transitions) for three different lengths,  $L_{SIW}$ ,

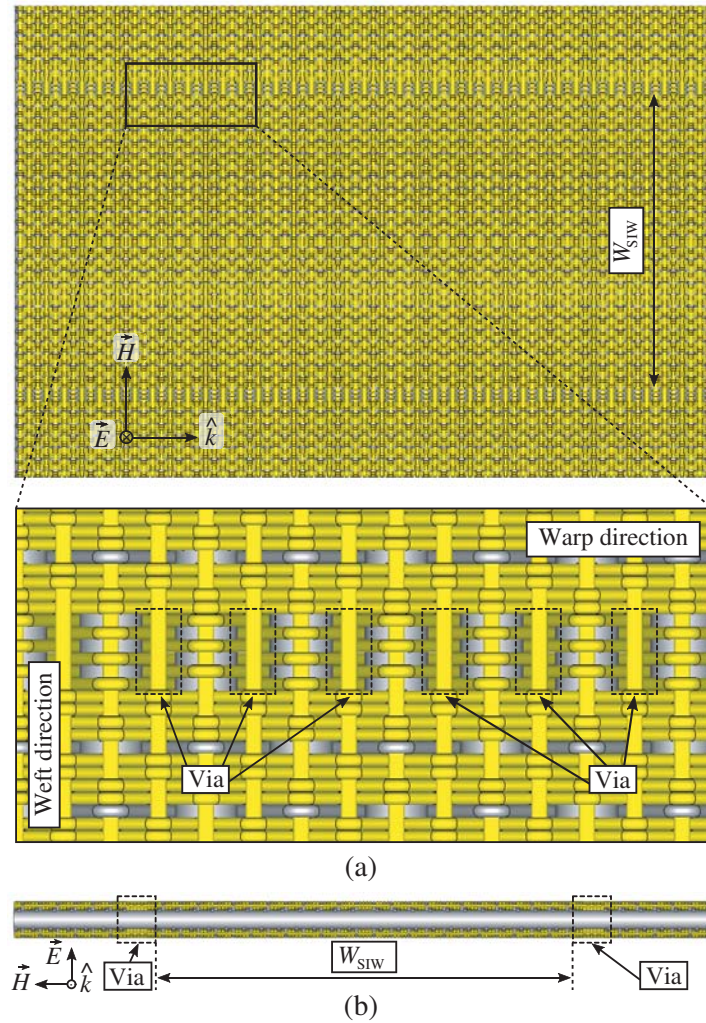


**Figure 5.** MM of the TIW (conductive material is yellow colored and dielectric materials are gray colored). (a) General top view and magnification. (b) General front view (port view).

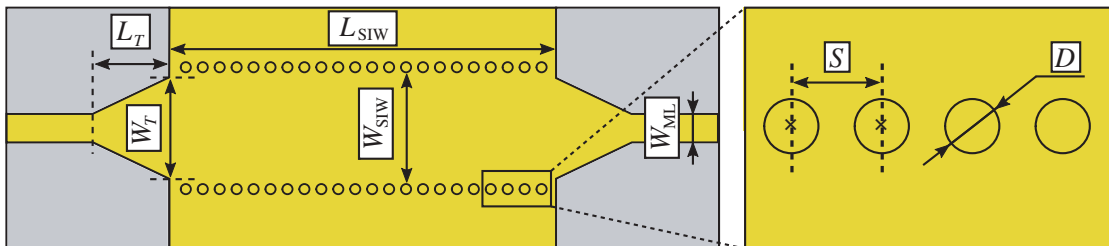


**Figure 6.** Schematic top view of the back to back TIW to microstrip transition, dimensions and magnification of the conductive vias.

of the prototype corresponding to 10, 15 and 20 mm, respectively. Although the simulated magnitude of the return losses is 0.35 dB/cm, it could be improved using silver threads in order to achieve a higher equivalent conductivity. The MM has not been completely simulated for the aforementioned lengths due to the computational resources required for this purpose.

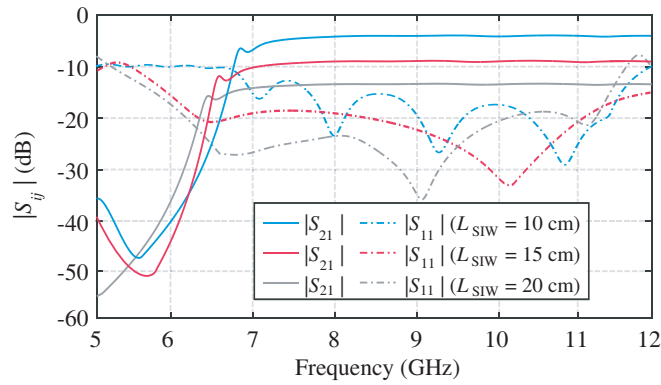


Figure 7. Simulated scattering parameters of the LM for the three different lengths.

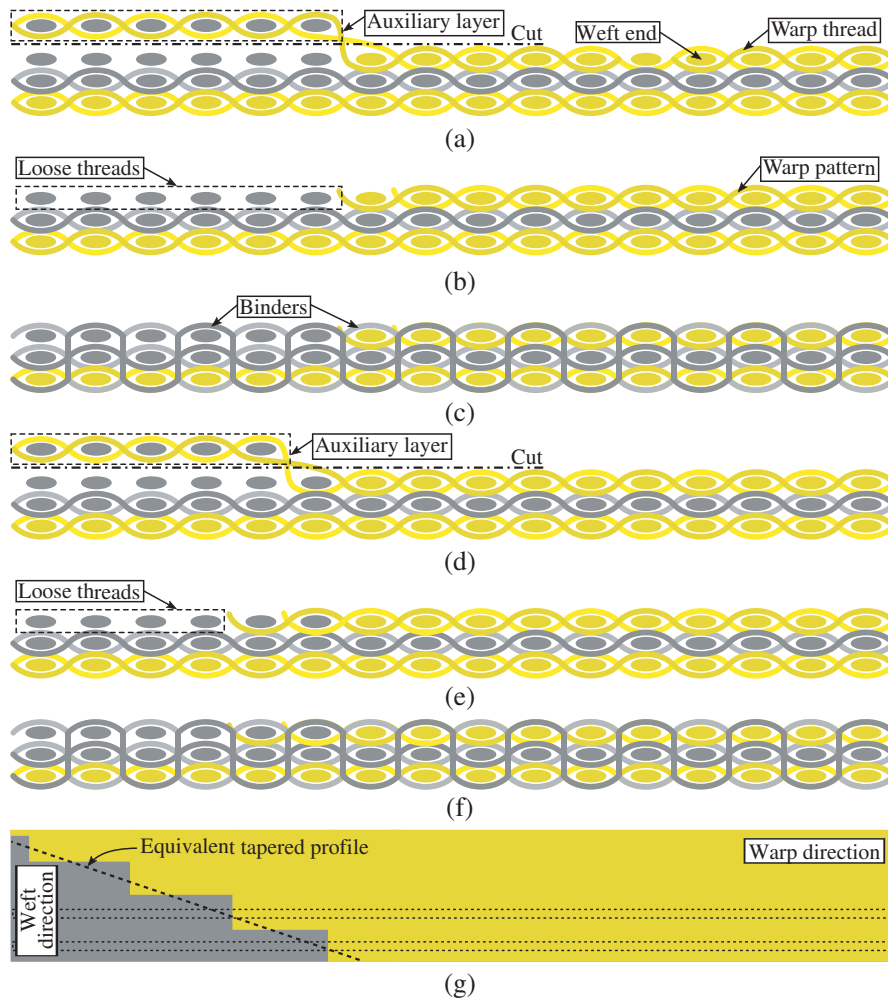


Figure 8. Schematic drawing of the woven structure based on a fully interlaced 3D fabric. (a) Side view of the woven structure using an auxiliary layer. (b) Side view of the woven structure with the loose threads, after cutting the auxiliary layer. (c) Side view of the woven structure using binders to avoid the loose threads. (d) Side view of the woven structure using the auxiliary layer for a different part of the tapered structure. (e) Side view of the woven structure with the loose threads, after cutting the auxiliary layer in (d). (f) Side view of the woven structure using binders to avoid the loose threads in (e). (g) Top view equivalence and details of the tapered profile and the two different parts of the taper.

## 8. FABRICATION PROCESS

Different TIWs have been manufactured using an industrial MüGrip loom, corresponding to different lengths, to validate the proposed TIW. In order to manufacture the woven TIW to microstrip transitions, not only three layers of warp and weft threads but also an auxiliary fourth layer of weft threads are required. The purpose of this extra layer is weaving the leftover conductive warp threads which are not required in the top layer of the tapered microstrip line. Once these conductive warp threads are woven in the auxiliary layer, a cutting process automatically cuts and removes this layer, leading to loose weft threads in the top layer. To avoid this problem, a warp pattern composed of dielectric threads called binders connecting all the layers achieves a compact structure. The before-mentioned process is summarised in Figure 8.

With the aim of achieving the tapered structure for the TIW to microstrip transitions, the conductive warp threads of the top layer must be interrupted. Figure 8(a) and Figure 8(d) depict the auxiliary layer corresponding to two different positions in the  $X$ -axis of the taper, respectively, as indicated in Figure 8(g). Likewise, Figure 8(b) and Figure 8(e) represent the loose threads after the cutting process for the two different positions of the taper. Figure 8(c) and Figure 8(f) depict the dielectric binders required to connect the three layers achieving a compact woven structure. Consequently, the taper becomes a stepped structure as depicted in Figure 8(g).

Once the auxiliary layer is removed, the prototype is manufactured. Figure 9 represents the top view of the manufactured TIW and magnification where a row of vias can be identified. Figure 10(a) depicts a side view of the proposed TIW and a magnification. The width of the woven structure,  $H_{SIW}$ , can be identified, as well as the separation between two consecutive dielectric weft threads, therefore, the separation between two adjacent conductive vias,  $S$ . Figure 10(b) represents the top view of the complete TIW, including the transitions to microstrip lines.

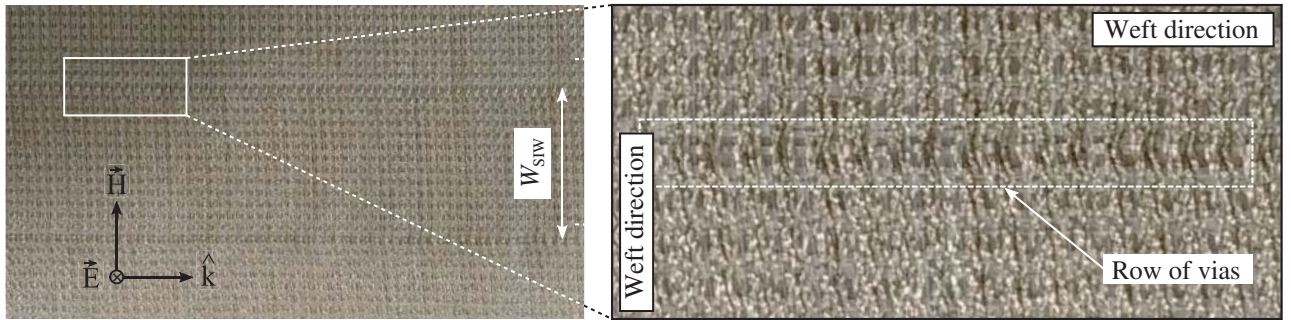


**Figure 9.** Top view of the manufactured TIW prototype and magnification.

## 9. EXPERIMENTAL VALIDATION

The prototype has been validated using the experimental setup presented in Figure 11. The two ports of the TIW section are connected to an Agilent N5247A PNA-X vector network analyser. Figure 12(a) represents a comparison between the simulated and measured insertion losses of the TIW for three different values of  $L_{SIW}$ , 10, 15 and 20 cm, respectively. For the simulations, the data associated with the LM have been considered. Figure 12(b) depicts a comparison between the simulated and measured return losses of the TIW.

As predicted by the simulations, the prototype presents a minimum insertion loss of 0.35 dB/cm, although it also presents a maximum insertion loss of 0.7 dB/cm, due to the ohmic losses of the conductive materials and the intrinsic radiative losses of the microstrip line. The insertion loss may be reduced using threads with higher conductivity. The use of coated threads may also lead to deterioration of the conductive coating, due to the wear out, consequently decreasing the thickness of the coating. For this reason, monofilament silver threads are proposed to achieve a higher conductivity while avoiding the uncoating problem due to the wear out.

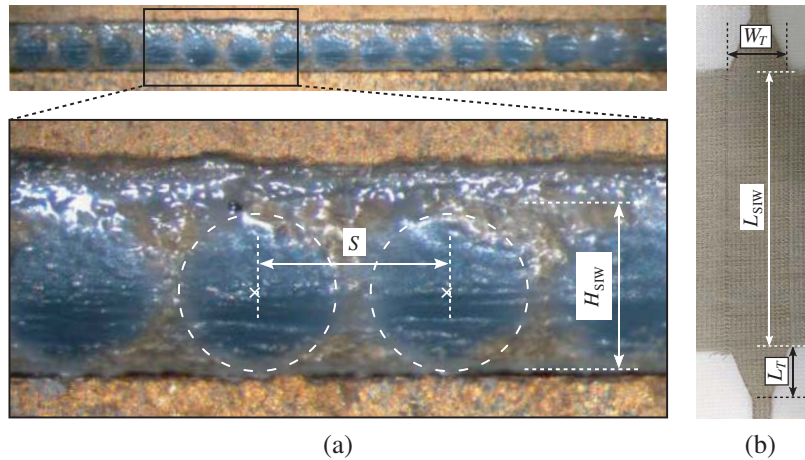


**Figure 10.** Overview of the manufactured prototype. (a) Side view and magnification. (b) Top view.

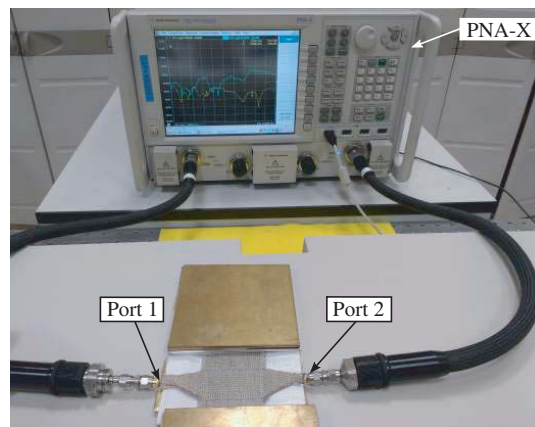


**Figure 11.** Set-up for the experimental validation of the TIW.

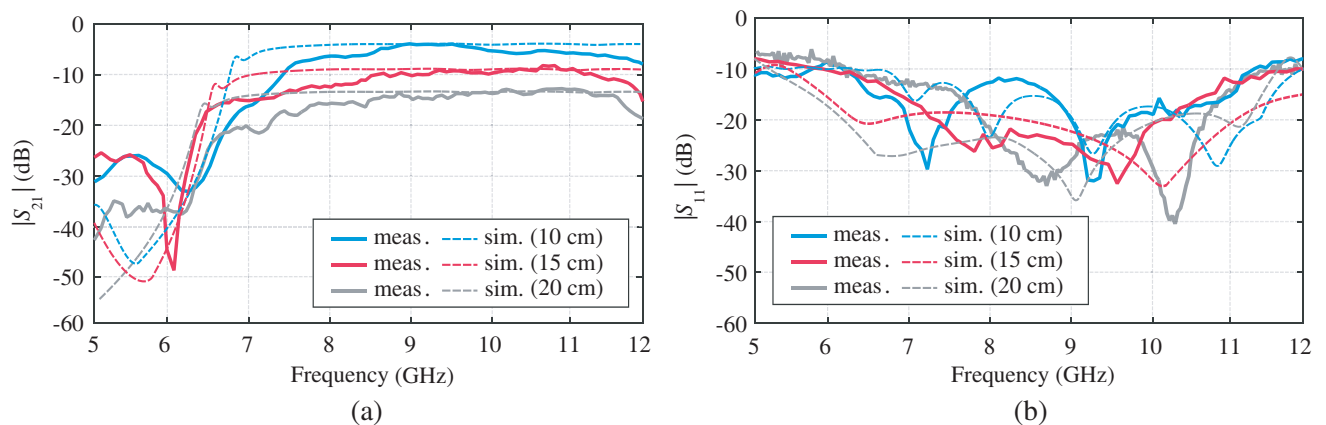


**Figure 12.** Simulated and measured scattering parameters of the TIW. (a)  $|S_{21}|$ . (b)  $|S_{11}|$ .

The agreement between simulated data and measurements demonstrates the validity of the TIW as a fully woven guiding structure. However, the differences between the simulated data and measured results may be due to manufacturing errors as well as the difficulty of fixing the connector in the textile structure.

## 10. CONCLUSIONS

A novel technique to develop microwave TIW using rigid weft threads has been presented. The general procedure based on the three-step parametric modelling to simulate woven structures presented [29] has been particularised to monofilaments, leading to a simplified two-step modelling. This two-step modelling has been applied to the design of the TIW. With the aim of achieving a complete integration of the prototype in textile for its experimental validation, a pair of tapered TIW to microstrip transitions has been designed and manufactured using an extra layer of textile materials.

To validate the design, three prototypes with different lengths have been experimentally characterised. The theoretically predicted behaviour of the textile structure has been experimentally verified. However, in order to reduce the insertion losses, it is proposed to use conductive threads with a lower resistance, such as silver monofilaments. Consequently, propagating waves through a woven waveguide has been demonstrated, opening a new field of research regarding TIW antennas based on SIW structures such as resonant cavities.

## ACKNOWLEDGMENT

This work has been supported by Gobierno de España TEC2015-72110-EXP, TEC2016-80815-P and FPU14/00016 grant, and by the Gobierno del Principado de Asturias (PCTI)/FEDER-FSE under projects IDI/2016/000372 and IDI/2017/000083.

## REFERENCES

1. DicCbshfsE, J., M. K. Abd Rahim, N. A. Samsuri, H. A. M. Salim, and M. F. Ali, "Embroidered fully textile wearable antenna for medical monitoring applications," *Progress In Electromagnetics Research*, Vol. 117, 321–337, 2011.
2. Ginestet, G., et al., "Embroidered antenna-microchip interconnections and contour antennas in passive UHF RFID textile tags," *IEEE Antennas Wireless and Propagation Letters*, Vol. 16, 1205–1208, Nov. 2017.
3. Paraskevopoulos, A., et al., "Higher-mode textile patch antenna with embroidered vias for on-body communication," *IET Microwaves, Antennas and Propagation*, Vol. 10, No. 7, 802–807, May 2016.
4. Kiourti, A., C. Lee, and J. L. Volakis, "Fabrication of textile antennas and circuits with 0.1 mm precision," *IEEE Antennas and Wireless Propagation Letters*, Vol. 15, 151–153, May 2016.
5. Wang, Z., L. Zhang, Y. Bayram, and J. L. Volakis, "Embroidered conductive fibers on polymer composite for conformal antennas," *IEEE Transactions on Antennas and Propagation*, Vol. 60, No. 9, 4141–4147, Sep. 2012.
6. Acti, T., et al., "Embroidered wire dipole antennas using novel copper yarns," *IEEE Antennas and Wireless Propagation Letters*, Vol. 14, 638–641, Nov. 2015.
7. Senbokuya, Y. and H. Tsunoda, "A study on the circular patch antennas using conductive non-woven fiber fabrics," *IEEE Antennas and Propagation Society International Symposium*, San Antonio, TX, USA, Jun. 16–21, 2002.
8. Monti, G., L. Corchia, E. De Benedetto, and L. Tarricone, "Wearable logo-antenna for GPS/GSM-based tracking systems," *IET Microwaves, Antennas and Propagation*, Vol. 10, No. 12, 1332–1338, Sep. 2016.
9. Shawl, R. K., B. R. Longj, D. H. Werner, and A. Gavrin, "The characterization of conductive textile materials intended for radio frequency applications," *IEEE Antennas and Propagation Magazine*, Vol. 49, No. 3, 28–40, Jun. 2007.
10. Jalil, M. E. B., M. K. Abd Rahim, N. A. Samsuri, N. A. Murad, H. A. Majid, K. Kamardin, and M. Azfar Abdullah, "Fractal koch multiband textile antenna performance with bending, wet conditions and on the human body," *Progress In Electromagnetics Research*, Vol. 140, 633–652, 2013.
11. Jais, M. I., M. F. B. Jamlos, M. Jusoh, T. Sabapathy, M. R. Kamarudin, R. B. Ahmad, A. Abdullah Al-Hadi, E. I. Bin Azmi, P. J. Soh, G. A. E. Vandenbosch, and N. L. K. Ishak, "A novel

- 2.45 GHz switchable beam textile antenna (SBTA) for outdoor wireless body area network (WBAN) applications,” *Progress In Electromagnetics Research*, Vol. 138, 613–627, 2013.
12. Soh, P. J., S. J. Boyes, G. A. E. Vandenbosch, Y. Huang, and S. L. Ooi, “On-body characterization of dual-band all-textile PIFA,” *Progress In Electromagnetics Research*, Vol. 129, 517–539, 2012.
  13. Lin, X., B. C. Seet, and F. Joseph, “Fabric antenna with body temperature sensing for BAN applications over 5G wireless systems,” *International Conference on Sensing Technologies*, Auckland, New Zealand, Dec. 8–10, 2015.
  14. Yahya, R., M. R. Kamarudin, N. Seman, and H. U. Iddi, “Eye shaped fabric antenna for UWB application,” *IEEE Antennas and Propagation Society International Symposium*, Orlando, FL, Jul. 7–13, 2013.
  15. Elmobarak Elobaid, H. A., S. K. Abdul Rahim, M. Himdi, X. Castel, and M. Abedian Kasgari, “A transparent and flexible polymer-fabric tissue UWB antenna for future wireless networks,” *IEEE Antennas and Wireless Propagation Letters*, Vol. 16, 1333–1336, Dec. 2016.
  16. Whittow, W. G., et al., “Inkjet-printed microstrip patch antennas realized on textile for wearable applications,” *IEEE Antennas and Wireless Propagation Letters*, Vol. 13, 71–74, Jan. 2014.
  17. Chauraya, A., et al., “Inkjet printed dipole antennas on textiles for wearable communications,” *IET Microwaves, Antennas and Propagation*, Vol. 7, No. 9, 760–767, Jun. 2013.
  18. Scarpello, M. L., I. Kazani, C. Hertleer, H. Rogier, and D. Vande Ginste, “Stability and efficiency of screen-printed wearable and washable antennas,” *IEEE Antennas and Wireless Propagation Letters*, Vol. 11, 838–841, Jul. 2012.
  19. Akbari, M., L. Sydänheimo, Y. Rahmat-Sami, J. Virkki, and L. Ukkonen, “Implementation and performance evaluation of graphene-based passive UHF RFID textile tags,” *International Symposium on Electromagnetic Theory*, Espoo, Finland, Aug. 14–18, 2016.
  20. Georget, E., R. Abdeddaim, and P. Sabouroux, “Analytical, simulation and measurement studies of a dual-band open-sleeve curved meander line antenna on a flexible substrate,” *Progress In Electromagnetics Research*, Vol. 145, 49–57, 2014.
  21. Hong, Y., J. Tak, and J. Choi, “An all-textile SIW cavity-backed circular ring-slot antenna for WBAN applications,” *IEEE Antennas and Wireless Propagation Letters*, Vol. 15, 1995–1999, 2016.
  22. Castel, T., et al., “Capacity of broadband body-to-body channels between firefighters wearing textile SIW antennas,” *IEEE Transactions on Antennas and Propagation*, Vol. 64, No. 5, 1918–1931, May 2016.
  23. Moro, R., et al., “Textile microwave components in substrate integrated waveguide technology,” *IEEE Transactions on Microwave Theory and Techniques*, Vol. 63, No. 2, 422–432, Feb. 2015.
  24. Bozzi, M., et al., “Innovative SIW components on paper, textile, and 3D-printed substrates for the Internet of Things,” *Asia-Pacific Microwave Conference (APMC)*, Nanjing, China, Dec. 6–9, 2015.
  25. Moro, R., et al., “Compact cavity-backed antenna on textile in substrate integrated waveguide (SIW) technology,” *European Microwave Conference*, 1007–1010, Nuremberg, 2013.
  26. Moro, R., et al., “Circularly-polarised cavity-backed wearable antenna in SIW technology,” *IET Microwaves, Antennas and Propagation*, Vol. 12, No. 1, 127–131, Oct. 2018.
  27. Yan, S., P. J. Soh, and G. A. E. Vandenbosch, “Dual-band textile MIMO antenna based on substrate-integrated waveguide (SIW) technology,” *IEEE Transactions on Antennas and Propagation*, Vol. 63, No. 11, 4640–4647, Nov. 2015.
  28. Alonso, L., et al., “Millimetre wave textile integrated waveguide beamforming antenna for radar applications,” *Global Symposium on Millimeter-Waves*, Montreal, QC, May 25–27, 2015.
  29. Alonso-González, L., et al., “On the techniques to develop millimeter-wave textile integrated waveguides using rigid warp threads,” *IEEE Transactions on Microwave Theory and Techniques*, Vol. 66, No. 2, 751–761, Feb. 2018.
  30. Alonso-González, L., et al., “Fully textile-integrated microstrip-fed slot antenna for dedicated short-range communications,” *IEEE Transactions on Antennas and Propagation*, Vol. 66, No. 5, 2262–2270, May 2018.

31. Hu, J., "Structure and mechanics of woven fabrics," *Woodhead Publishing in Textiles, The Textile Institute*, 63–66, New York, NY, USA, 2004.
32. Chao, L., B. Yu, A. Sharma, and M. N. Afsar, "Dielectric permittivity measurements of thin films at microwave and terahertz frequencies," *European Microwave Conference*, Manchester, UK, Oct. 10–13, 2011.
33. Steele, B. C., "Electronic ceramics," *Elsevier Applied Science*, 140, London, UK, USA, 1991.
34. Bilisik, K., N. S. Karaduman, N. E. Bilisik, and H. E. Bilisik, "Three-dimensional fully interlaced woven preforms for composites," *Textile Research Journal*, Vol. 83, No. 19, 2060–2084, 2013.
35. Ma, P. and Z. Gao, "A review on the impact tension behaviors of textile structural composites," *Journal of Industrial Textiles*, Vol. 44, No. 4, 572–604, 2015.